

## Quantitative chemical mapping of sodium acrylate- and N-vinylpyrrolidone-enhanced alginate microcapsules

TOHRU ARAKI<sup>1</sup>, ADAM P. HITCHCOCK<sup>1</sup>, FENG SHEN<sup>2</sup>,  
PATRICIA L. CHANG<sup>2,\*</sup>, MAGGIE WANG<sup>1</sup> and RONALD F. CHILDS<sup>1</sup>

<sup>1</sup>Department of Chemistry, McMaster University, Hamilton, Ontario, Canada

<sup>2</sup>Department of Pediatrics, McMaster University, Health Sciences Centre Room 3H31,  
McMaster University, 1200 Main St. West, Hamilton, Ontario, Canada L8N 3Z5

Received 10 May 2004; accepted 10 September 2004

**Abstract**—Alginate microcapsules enclosing recombinant cells secreting therapeutic products have been used successfully to treat several murine models of human diseases. The mechanical and chemical properties of these alginate capsules can be improved by the addition and *in situ* photopolymerization of sodium acrylate and N-vinylpyrrolidone in the alginate capsule. The purpose of this modification was to form additional covalent cross-links. In this work we have used scanning transmission X-ray microscopy (STXM) to probe the nature and location of the chemical modifications in the modified capsules by comparison with unmodified capsules. Analysis of X-ray image sequences and selected area spectra has been used to map the calcium gradient in capsules, to identify the presence of polyacrylate throughout the capsules and the localization of poly-N-vinylpyrrolidone in the outer regions of the alginate capsules. The differences in the spatial distributions of these species have led to better understanding of the chemical modifications that provide a mechanically more stable capsule structure.

*Key words*: Molecular imaging; co-polymer; hydrogel; image analysis; photopolymerization.

### INTRODUCTION

The concept of implanting biological products enclosed in permeable membrane capsules was first described by Chang [1] and has been proven effective in the encapsulation of non-autologous pancreatic islet cells [2], hepatocytes [3] and other cultured cells [4]. The technology has been extended to the encapsulation of genetically modified cells as an alternative approach to gene therapy by delivering desired therapeutic proteins [5–13]. The clinical efficacy of this new form of

---

\*To whom correspondence should be addressed. Tel.: (1-905) 525-9140, ext. 22280. Fax: (1-905) 524-5707. E-mail: changp@mcmaster.ca

therapy was first demonstrated when capsules containing cells secreting mouse growth hormone were implanted into mutant dwarf mice. These dwarf mice gained  $> 25\%$  of their body weights after one month of implantation [8]. The success of the strategy has been replicated in a variety of models of human diseases such as Huntington's disease [14], ALS [15], lysosomal storage disease [11, 12], hemophilia [10] and cancer [13, 16, 17].

The microcapsules most commonly used consist of an alginate central core with poly-L-lysine and alginate layers surrounding the core (APA) capsules [18]. While these capsules have many desirable properties, they suffer from a lack of long term stability when implanted in larger animals such as dogs [19]. Several approaches have been made to enhance the strength of the APA capsules [20–22]. One technique that we have developed involves the treatment of the initially formed capsule with a dilute solution of sodium acrylate (SA) and N-vinylpyrrolidone (NVP) in such a manner that these monomers undergo polymerization with cross-linking to the calcium alginate forming the capsule [23, 24]. This simple technique greatly strengthens the final APA capsules without significantly affecting cell survival during the encapsulation process.

In this paper we address the issue of the distribution of SA and NVP within capsules made by this new methodology. This is a difficult problem to resolve as the concentrations of the added monomers are low and the capsules are very susceptible to collapse on loss of water. Analytical electron microscopes have excellent spatial resolution for morphological studies of capsules and can provide low sensitivity elemental analysis through energy-dispersive X-ray microanalysis [25]. However, they do not differentiate species with similar elemental composition and do not have the sensitivity required for the direct detection of minor components such as the SA and NVP species in this system. Furthermore, radiation damage is a significant problem when using high energy electron beams to study fragile polymers.

Scanning transmission X-ray microscopy (STXM) is an emerging synchrotron-based technique [26, 27] that is a very powerful tool for imaging and quantitative, spatially resolved chemical mapping of heterogeneous soft materials such as polymers [28–31] and biomaterials [32–34]. It has been used to detect directly the chemical composition and morphology of core–shell microspheres and structured gels [35, 36]. Here we report on the application of this analytical approach to study the molecular changes occurring in the covalently modified alginate microcapsules, thus providing insight into the chemical basis for the improved stability observed.

Previous microchemical studies of alginate capsules have shown clearly the role of Ca replacement of Na to form the ionically cross-linked shell that forms the capsule boundary [37, 38]. As described below, STXM readily determines this feature and provides high spatial resolution mapping of the Ca distribution in the region of the edge and at reduced spatial sampling all across the approx. 500- $\mu\text{m}$ -diameter capsules.

## MATERIALS AND METHODS

### *Materials*

Sodium alginate (Keltone), a gift from NutraSweet Kelco (San Diego, CA, USA), has a fine mesh size (approx. 150 kDa), low viscosity (10–60 mPa S) and molecular mass of 428 kDa when measured by gel-permeation chromatography (GPC). Acrylic acid (AA), sodium acrylate (SA) and N-vinyl-pyrrolidone (NVP) were purchased from Aldrich (Milwaukee, WI, USA). Hydroxy-1-[4-(hydroxyethoxy)phenyl]-2-methyl-1-propanone (Irgacure<sup>®</sup> 2959) was purchased from Ciba (Mississauga, ON, Canada). Poly-L-lysine (PLL, molecular mass 15–30 kDa) was from Sigma (Mississauga, ON, Canada), Trypan blue from Gibco Industries (Los Angeles, CA, USA) and sodium citrate from Bioshop Canada (Burlington, ON, Canada). Serum-free media (SFM) was purchased from Gibco (Mississauga, ON, Canada).

### *Alginate capsule fabrication*

This was as described by Ross *et al.* [11]. Briefly, a 1.5% solution of sterile-filtered sodium alginate was extruded through a 27 gauge needle with concentric air flow using a modified Orion Sage syringe. The droplets were collected in a 1.1% calcium chloride bath in which calcium ions cross-linked the alginate molecules. These alginate beads were used for the chemical modification with poly(SA/NVP) and for the STXM study. For the preparation of the classical APA capsules, the alginate beads were coated with PLL and then with 0.03% alginate before washing with saline as described [11]. All solutions were at neutral pH.

*Poly(SA/NVP) modification of alginate capsules.* A solution containing 200  $\mu$ l 0.2% Irgacure 2959, 60  $\mu$ l 1.39 M SA in saline and 100  $\mu$ l 0.834 M NVP in saline was added to 2 ml of alginate beads fabricated as described above, but before coating with PLL and alginate (each ml containing approx. 4000 microcapsules) in 0.5 ml saline in a culture dish. This ratio of reagents corresponded to approx. 20% modification, based on the molar ratio of SA to alginate. The molar ratio of SA to NVP was kept constant at 1 : 1 ratio [23]. After a gentle shaking, the beads were exposed to UV light for 30 min on an ice bath. The resulting beads were transferred into saline for storage prior to preparation for STXM measurements, or coated with PLL and then with 0.03% alginate. In addition to the standard recipe (100%) special capsules were fabricated with a threefold increase in the SA and NVP concentrations (300%).

### *Section preparation for STXM*

Optimal thickness for transmission measurements in the C<sub>1s</sub> region are about 100 nm of unit density organic matter. Since the alginate capsules had very low density, the capsules were cut to form sections of enough thickness to provide adequate absorbance. Prior to cryo-microtoming, the modified alginate capsules

were gradually dehydrated by being transferred to 10%, 30%, 50%, 70%, 90%, 95%, 100% ethanol solutions for 15 min at each concentration. The dehydrated beads were frozen with liquid nitrogen and cryo-microtomed to either approx. 250 nm or approx. 1  $\mu\text{m}$  thickness. The sample was warmed to room temperature, the ethanol used for cryomicrotomy evaporated and the sample was examined in that state.

*STXM measurements.* Soft X-ray spectroscopy and NEXAFS (near-edge X-ray absorption fine structure) imaging was carried out using a newly commissioned, interferometrically controlled, scanning transmission X-ray microscope [39] on beamline 5.3.2 [40] at the Advanced Light Source (Berkeley, CA, USA). Measurements were made at the  $\text{C}_{1s}$  edge (280–320 eV),  $\text{Ca}_{2p}$  edge (340–365 eV),  $\text{N}_{1s}$  edge (390–420 eV) and  $\text{O}_{1s}$  edge (525–565 eV). STXM was used analytically by acquiring NEXAFS spectra at a single location, collecting line scan spectra, or collecting a sequences of images through the core edge of interest. The image sequence data was converted to component maps (distributions of distinct chemical species, such as proteins, polysaccharides, nucleic acids, etc.) by spectral fitting using linear regression procedures [35, 36]. Reference spectra for the fitting were measured with the STXM532 instrument from pure samples of the individual components. The latter samples were prepared by solvent casting a dilute solution of each species (polyacrylate, poly-N-vinylpyrrolidone, alginate) on to 100 nm  $\text{Si}_3\text{N}_4$  windows to form a deposit with micron or larger sized regions of 100–200 nm thickness from which the reference spectra were obtained. The image and spectral processing was carried out using the aXis2000 package (available from <http://unicorn.mcmaster.ca/aXis2000.html>), which is coded in Interactive Data Language (IDL, Research Systems).

### *EDTA dissolution*

Two kinds of microcapsules were compared for their stability in the presence of EDTA: standard calcium alginate microcapsules and 10% AA/NVP-modified microcapsules. 40  $\mu\text{l}$  of the capsules was placed in 200  $\mu\text{l}$  sodium EDTA (0.17 M). Capsule size and the number remaining intact were monitored over time using a Wilde M40 light microscope.

*Microcapsules calcium content measurements.* Ca content was measured with an ICP-MS (inductively coupled plasma source mass spectrometer) consisting of a quadrupole mass spectrometer with inductively coupled argon plasma as an ion source (Perkin-Elmer Elan 6100). Liquids introduced into the plasma were ionized and then passed to the mass spectrometer through a two-stage ion extraction interface. The microcapsules were made as previously described, washed four times with doubly distilled water to remove the free calcium and 70  $\mu\text{l}$  capsules was placed in 1 ml 20 mM EDTA to chelate calcium cations for 40 min until all capsules

disintegrated. 100  $\mu\text{l}$  1%  $\text{H}_2\text{O}_2$  was added to digest the solutes and to enhance the measurement of ion intensity. The EDTA solution was diluted with 10 ml doubly distilled water before analysis. A blank sample was made from the mixture of equal amounts of EDTA,  $\text{H}_2\text{O}_2$  and DD- $\text{H}_2\text{O}$  as a reference.

The liquid samples were introduced into the argon plasma at 1.0 ml/min using a peristaltic pump to the nebulizer where the sample aerosol was formed. A calibration curve was constructed from seven standard samples with varying calcium concentrations at 0, 20, 100, 500, 1000, 3000 and 10 000 ppb.

The theoretical calcium concentration of each microcapsule type was measured by the change of conductivity in calcium chloride solution before and after gelation. Microcapsules were made with 5 ml 1.5% alginate solution extruded into 20 ml 1.1%  $\text{CaCl}_2$ . The conductivities of alginate capsules solution were measured at 30 min, 60 min, 2 h and 12 h after gelation. A calibration curve was obtained with five concentrations of  $\text{CaCl}_2$  in DI- $\text{H}_2\text{O}$ : 1.0%, 0.8%, 0.6%, 0.4% and 0.2%. The conductivity of  $\text{Ca}^{2+}$  in solution was measured with an Orion 105 conductivity meter.

## RESULTS

### *Capsule mechanical properties*

Standard APA and NVP/SA-modified capsules appeared to be very similar under low-power phase contrast microscopy (Fig. 1A and 1C). A hydrogel dissolution assay was carried out to examine the stability of the modified alginate microcapsules on depletion of the initial ionic cross-linking by the divalent cation calcium. Since EDTA is a strong chelating agent and can remove  $\text{Ca}^{2+}$ , it was added to the two types of capsules, and the time taken for capsule disintegration was measured (Fig. 1B and 1D). Alginate microcapsules that were only calcium-cross-linked became translucent and difficult to visualize under light microscopy in 0.17 M EDTA in less than 1 min, indicating dissolution of the capsules (Fig. 1B). In contrast, capsules prepared with a 10% modification ratio of SA and NVP still appeared to be intact after the same amount of time (Fig. 1D).

### *$\text{Ca}^{2+}$ content of microcapsules*

In order to monitor changes in the concentration of  $\text{Ca}^{2+}$  in a microcapsule with time when in contact with a  $\text{CaCl}_2$  solution, changes in the conductivities of the solutions were measured. It is found that the conductivity of alginate capsules in contact with solution did not change with time (data not shown). This indicated that the concentration of  $\text{Ca}^{2+}$  binding to alginate reached equilibrium soon after gelation.

The AA-, SA- or NVP-modified calcium alginate microcapsules showed greatly enhanced levels of  $\text{Ca}^{2+}$  as compared to the unmodified capsules (Fig. 2). When the

capsules were modified with 20% NVP, the amount of  $\text{Ca}^{2+}$  present was increased by approx. 50%. However, when they were modified with 20% SA, the  $\text{Ca}^{2+}$  binding increased more than 4-fold.

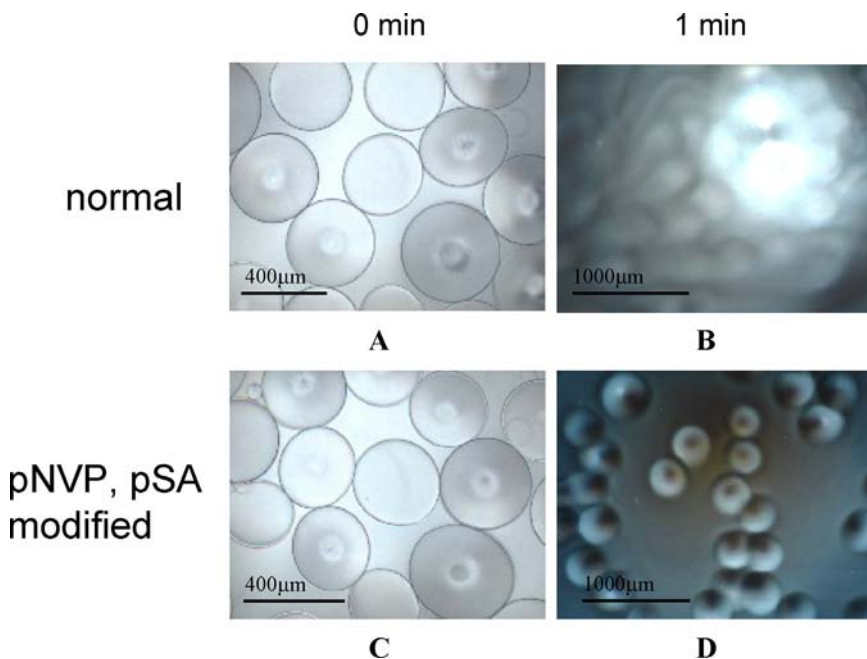


**Figure 1.** Phase-contrast microscope images of (A, B) classical APA beads and (C, D) NVP-modified microcapsules, before and after exposure for 1 min to a 0.17 M aqueous EDTA solution. Both sets of capsules were coated with PLL and SA. This figure is published in colour on <http://www.ingenta.com>

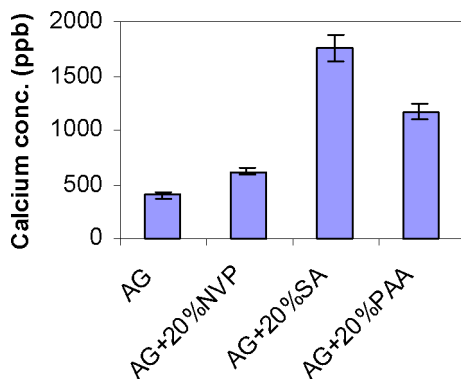


**Figure 2.** Calcium binding in modified microcapsules. A series of alginate capsules was prepared, incorporating NVP or SA or poly(acrylic acid) (PAA) and compared with the regular alginate capsules (AG) for their  $\text{Ca}^{2+}$  content. The capsules were dissolved in sodium-EDTA and the solutions were analyzed by ICP-MS for their calcium content. This figure is published in colour on <http://www.ingenta.com>

It has been reported by Desai [41] that the formation of an interpenetrating network (IPN) between the calcium alginate and calcium poly(acrylate) leads to an increase in  $\text{Ca}^{2+}$  content of capsules. As noted above, we also observed an increase in  $\text{Ca}^{2+}$  when the capsules were modified by the addition of PSA (Fig. 2). However, as we have shown previously [23], the formation of an IPN between alginate and poly(acrylate) does not lead to capsules with good long term strength. This indicates that the post capsule polymerization route in this work that uses sodium acrylate as the modifying monomer leads to capsules with a composition different from a simple IPN system.

### STXM analysis

The role of SA and NVP modification in capsule strengthening has been investigated with STXM by mapping the chemical composition of the capsules at high spatial resolution (approx. 50 nm). The quality of the analysis is closely linked to the ability of  $\text{C}_{1s}$  spectroscopy to differentiate the key species. Figure 3 presents the  $\text{C}_{1s}$  spectra of polySA, polyNVP and SA, the  $\text{Ca}_{2p}$  spectrum of calcium carbonate and the  $\text{N}_{1s}$  spectrum of NVP, which are used as reference spectra in the quantitative chemical analysis. It is clear that each species has a distinct  $\text{C}_{1s}$  spectrum, that the strong distinctive spin-orbit-split  $\text{Ca}_{2p}$  signal is extremely sensitive to Ca and that the  $\text{N}_{1s}$  edge will be specific to the NVP.  $\text{O}_{1s}$  spectra were also recorded (not shown), but

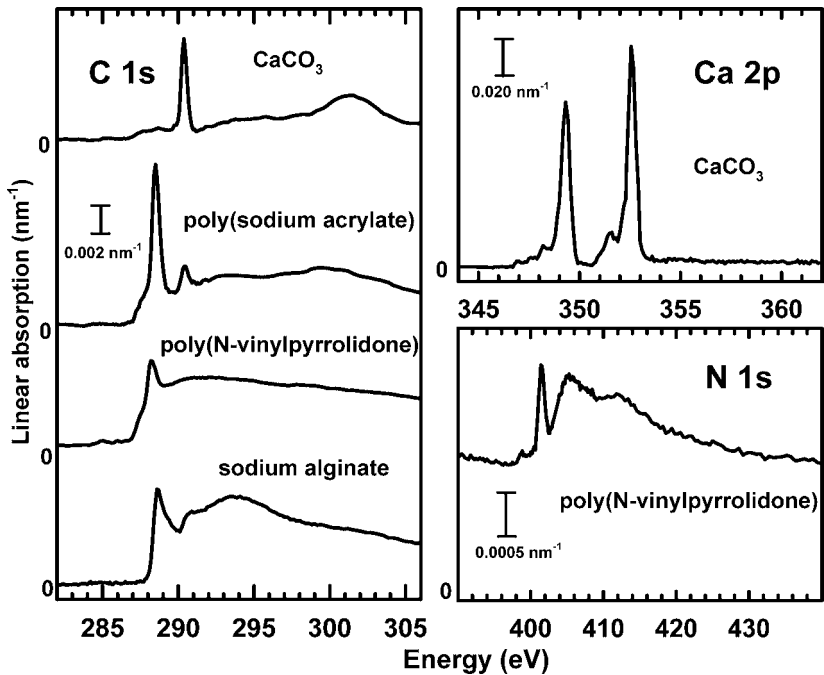


**Figure 3.** (Left)  $\text{C}_{1s}$  NEXAFS spectra of polySA, polyNVP and polyalginate. (Right)  $\text{Ca}_{2p}$  NEXAFS spectrum of carbonate and  $\text{N}_{1s}$  NEXAFS spectra of polyNVP.

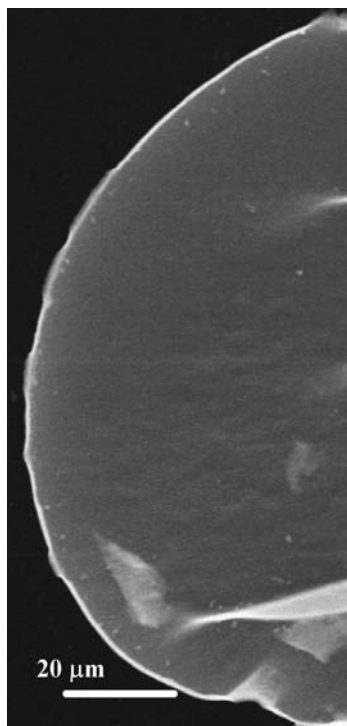


**Figure 4.** Optical density image ( $650 \times 1370$  pixels, 1 ms/pixel) recorded at 352.6 eV ( $\text{Ca}_{2p_{1/2}} \rightarrow 3d$  transition) of a cryo-cut NVP-modified alginate capsule. The sample was ethanol substituted, cryo-microtomed, placed on a 100-nm-thick  $\text{Si}_3\text{N}_4$  window and recorded in the dry state at room temperature.

we did not want to rely on use of this edge for the analysis, since the goal is to examine capsules in the wet state, where the  $\text{O}_{1s}$  absorption spectrum of the water would completely overwhelm the signal from the polymer species.

An image of a 1- $\mu\text{m}$ -thick section of about half of one of the polyNVP/polySA-strengthened capsules was recorded at 352.6 eV (peak of the  $\text{Ca}_{2p_{1/2}} \rightarrow 3d$  transition) (Fig. 4). The transmission signal has been converted to optical density using the signal in the adjacent empty region of the  $\text{Si}_3\text{N}_4$  window as the  $I_0$  signal. The enhanced density at the edges is associated with a higher amount of Ca ionic cross-linking in the initial formation of the capsule. The signal through the interior of the capsule is relatively constant at approx. 50% of the edge signal. The absence of signal outside the capsule and the uniformity of the capsule interior indicate the preparation of the microtomed sample is of very high quality, with only a few regions of the interior being folded, and about 15% of the edge, having suffered some mechanical damage.

The component maps of alginate, acrylate, NVP and alginate were derived from an image sequence recorded in the  $\text{C}_{1s}$ ,  $\text{Ca}_{2p}$ ,  $\text{N}_{1s}$  and  $\text{O}_{1s}$  edges. The sample was obtained from a cryo-section of 250 nm thick in the ethanol replaced frozen

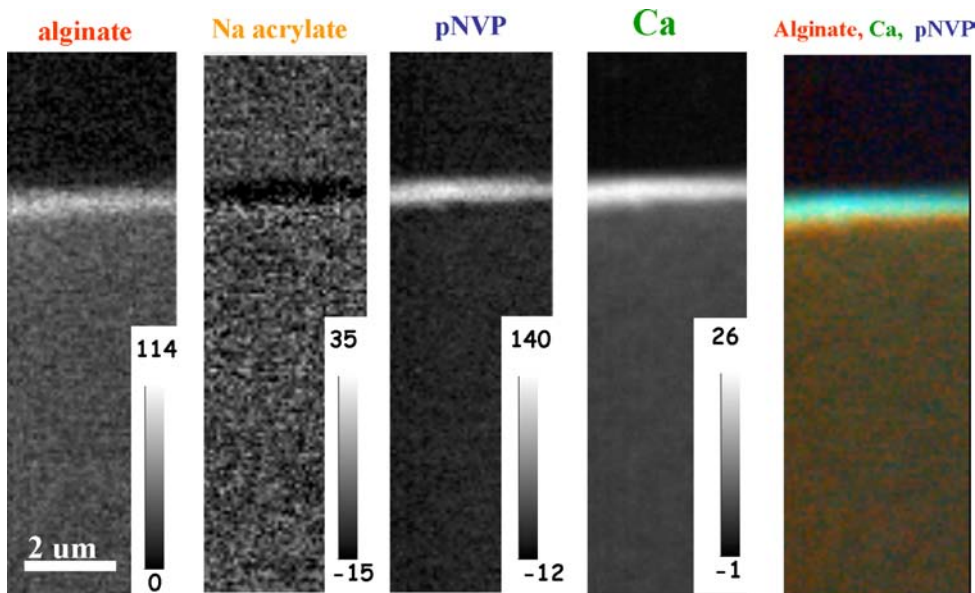


**Figure 5.** Component maps of alginate, acrylate, pNVP and Ca derived from a multi-edge image sequence ( $C_{1s}$ ,  $Ca_{2p}$ ,  $N_{1s}$ ,  $O_{1s}$ ). The reference spectra (Fig. 3) are on a linear absorption scale and, thus, the greyscale of the component maps is thickness in nm. The total thickness obtained by summing all components is about 140 nm at the edge and 50 nm in the centre, indicating an effective density in the centre of the capsule of the order of 5% (based on the 1- $\mu$ m setting for the cryo-microtomy used to prepare this sample). The color coded composite map on the right clearly shows the pNVP as sitting at and partly outside the Ca-rich edge. This figure is published in colour on <http://www.ingenta.com>

state, across the edge of an acrylate/NVP strengthened alginate capsule. The maps indicate a strong concentration of NVP and, to a lesser extent, alginate at the edge of the capsule, but do not show edge localization of the acrylate (Fig. 5).

The color-coded composite maps generated from component maps derived from  $C_{1s}$  image sequences of the edge region of 250-nm-thick dry sections prepared from an unmodified capsule and for three capsules with different processes of modification are shown in Fig. 6. Sample #1 was the unmodified capsule sample, #2 was modified with the NVP/SA procedure (100% modification), while capsules #3 and #4 were fabricated with using NVP or SA alone, respectively. The NVP signal (blue colour) was found to the greatest extent in #2, and in this sample, the density of NVP (the blue colour) was higher at the edge than further into the core of the capsule. The concentration of the NVP component derived from the analysis is approx. 20% of total thickness at the edge, decreasing to a negligible amount in the interior.

The component maps of alginate, acrylate and NVP derived from singular value decomposition (SVD) analysis [36] of a  $C_{1s}$  image sequence recorded at the edge of a dry, 250-nm-thick section of an alginate capsule strengthened with poly(acrylate/NVP) are shown in Fig. 7. The maps indicate a greater amount of

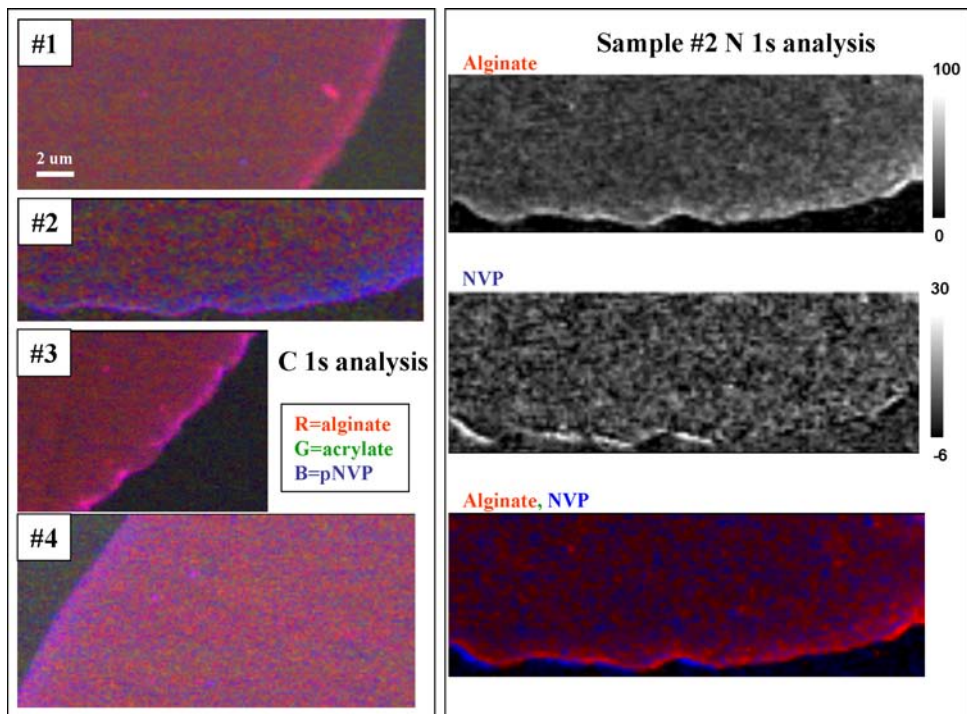


**Figure 6.** (Left) Composite chemical maps of the alginate (red), acrylate (green) and NPV (blue) components derived from  $C_{1s}$  image sequences for cryo-microtomed sections of 4 types of alginate capsules: #1, alginate beads (control); #2, alginate beads with NVP + acrylic acid + initiator + UV lighting; #3, alginate beads with NVP + initiator + UV lighting; #4, alginate beads with acrylic acid + initiator + UV lighting. The STXM samples were cryo-microtomed to 250 nm thickness, placed on the  $Si_3N_4$  windows and allowed to dry. (Right) Alginates (top) and NVP (middle) component maps derived from analysis of a  $N_{1s}$  image sequence of sample #2, along with color-coded composite (bottom). This figure is published in colour on <http://www.ingenta.com>

NVP (and alginate) at the edge of the capsule, but indicate that the acrylate is more uniformly distributed (at a low level) throughout the capsule (Fig. 7, left panel, top 3 images). The enhanced alginate signal localized at the edge is associated with the Ca ionic cross-linking. The NVP concentration at the edge suggests the polymerization is occurring preferentially at the edge, possibly due to differences in the diffusion of the neutral NVP and ionic SA through the capsule wall into the capsule. In order to demonstrate the spectroscopic basis for this analysis, the component maps were subjected to a threshold masking procedure to identify those pixels with strong signals of each species. The average spectrum of these pixels was then extracted (Fig. 7, left panel, bottom image) and compared to the spectra of the pure materials (Fig. 7, right panel). The right-hand panels of Fig. 7 show the resulting spectral comparison, along with a single energy image of the analysed region with superimposed colored spots which indicate the pixels of

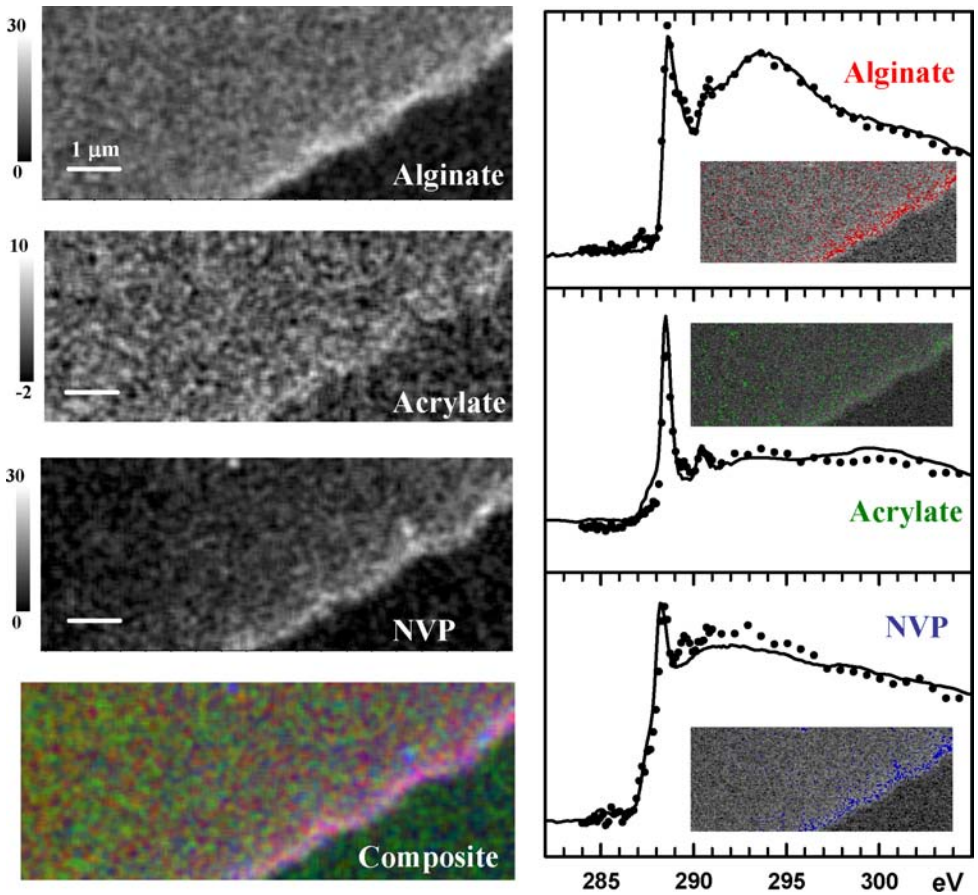


**Figure 7.** Component maps derived from C<sub>1s</sub> image sequence recorded from a normal concentration (100% modification) poly(acrylate/NVP)-strengthened alginate capsule. A 250-nm-thick-section was cryo-microtomed from ethanol-replaced capsules and allowed to dry on a Si<sub>3</sub>N<sub>4</sub> window. Left-hand panel: top 3 images are component maps of alginate, acrylate and NVP; bottom image is a color-coded composite (red = alginate, green = acrylate, blue = NVP). Right-hand panel: C<sub>1s</sub> spectra of selected pixels, regions of the 250—compared to the spectra of pure poly(acrylate), polyNVP and Ca<sup>2+</sup> cross-linked alginate. The selected pixels are those for which the equivalent thickness exceeded threshold values of 15, 7 and 20 nm for the alginate, acrylate and NVP component maps, respectively. This figure is published in colour on <http://www.ingenta.com>

high component content. This approach clearly indicates the spectral basis for the chemical analysis and highlights the enhanced concentration of NVP at the edge.

The same analyses were performed for the strengthened alginate capsules in which the NVP and acrylate concentrations corresponded to 300% modification (Fig. 8). Again, the component maps indicate edge enhancement of the alginate and NVP, but very little localization of the acrylate (Fig. 8, left panel, top 3 images). This is verified by comparison of the spectra of pixels of high component content derived from threshold masking the component maps (Fig. 8, left panel, bottom

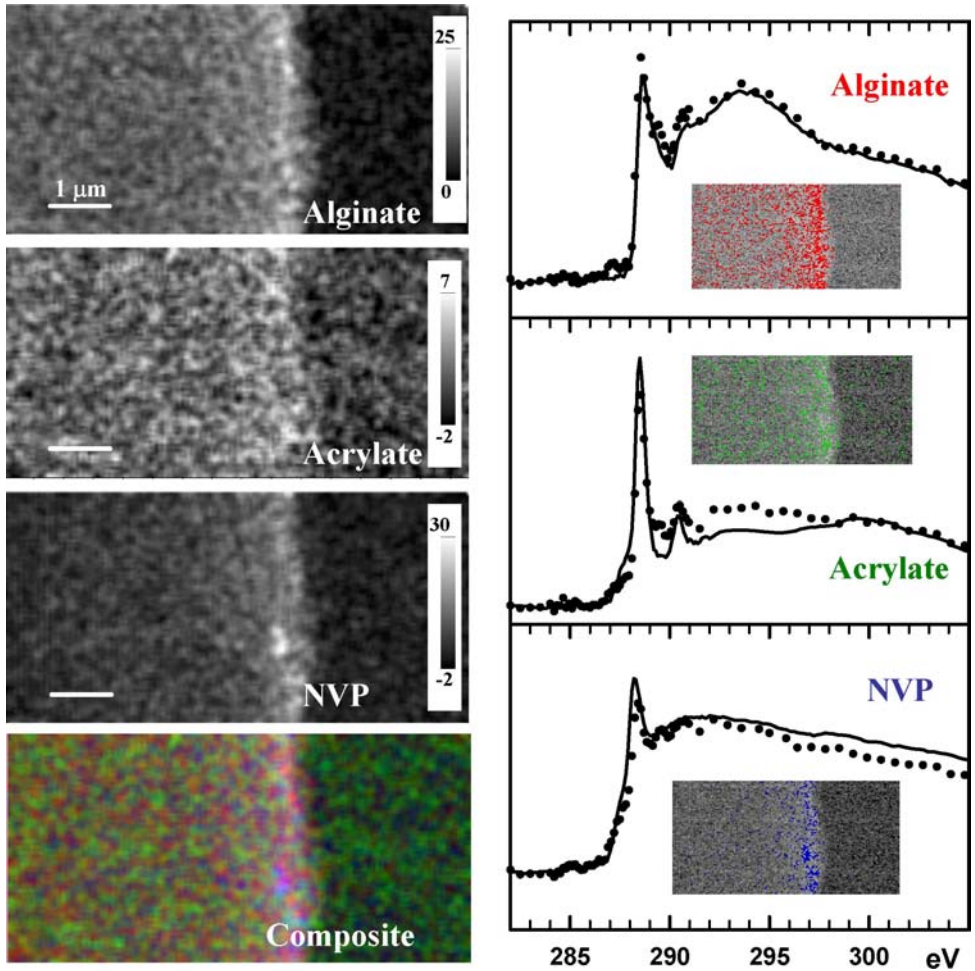


**Figure 8.** Component maps derived from  $C_{1s}$  image sequence recorded from an enhanced (300% modification) concentration poly(acrylate/NVP) strengthened alginate capsule. The 250-nm-thick section was cryo-microtomed from ethanol-replaced capsules and allowed to dry on a  $Si_3N_4$  window. Left-hand panel: top 3 images are component maps of alginate, acrylate and NVP; bottom image is a color-coded composite (red = alginate, green = acrylate, blue = NVP). Right-hand panel:  $C_{1s}$  spectra of selected pixels, compared to the spectra of pure poly(acrylate), polyNVP and  $Ca^{2+}$  cross-linked alginate. The selected pixels are those for which the equivalent thickness exceeded threshold values of 20, 10 and 20 nm for the alginate, acrylate and NVP component maps, respectively. This figure is published in colour on <http://www.ingenta.com>

image) with the spectra of the pure materials (Fig. 8, right panel). These pixels are predominantly at the edge for NVP, and to a lesser extent for alginate, but distributed more uniformly over the sampled regions for the acrylate.

The line profiles across the edge of the region measured in Fig. 5 are presented in Fig. 9. In the upper plot the vertical scale is thickness, while in the lower it is percent composition. The sum of all the component maps should be a good

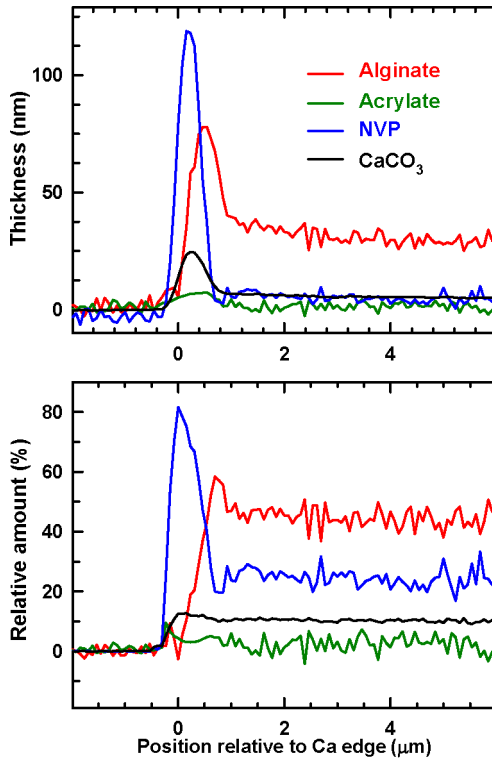


**Figure 9.** Line profiles from component maps of 5 across the edge of the capsule region. The top panel represents the thickness, and the bottom panel the percent composition of the various components relative to the Ca edge. This figure is published in colour on <http://www.ingenta.com>

approximation to the overall density through various regions of the capsule (the gray scales of the component maps actually indicate thickness, and this is the correct picture in the ‘collapsed’ dehydrated state. However, in the original cryo-microtomed section of the wet capsule the thickness is uniform and it is the density of the solid components in the gel that is varying). While the component densities vary as described above, when the ratio of these signals to the sum is taken in order to derive fractional composition, a slightly different picture emerges. It is clear that the NVP enhancement is quite localized at the outer parts of the edge-enhanced region.

From these and additional similar measurements, the results of STXM in the above studies indicate that:

- The capsules have enhanced density (two-fold) in the outer approx.  $0.5 \mu\text{m}$  of the capsule.
- The alginat density is relatively uniform in the interior of the capsule.
- The  $\text{Ca}^{2+}$  concentration falls off towards the capsule interior rather slowly and even the edge enhancement is a density increase much more than a compositional change.

- (d) There is clear evidence for the NVP to be concentrated in the edge region, coincident with the dense Ca-alginate region, and consistent indications that much of the NVP lies outside the originally formed Ca-alginate cross-linked capsule wall.
- (e) In contrast, the acrylate distribution is fairly uniformly distributed throughout at least the 10–20  $\mu\text{m}$  just inside the edge.

## DISCUSSION

The SA and NVP *in situ* polymerization methodology was thought to give capsules with enhanced properties compared to those formed by a simple interpenetrating network (IPN) of calcium alginate and calcium poly(acrylate) [20]. This suggests that, in addition to the radical polymerization of the vinyl monomers to form an IPN, hydrogen abstraction from the alginate is also taking place, resulting in covalent cross-linking of the alginate. The low concentrations of the added monomers and the sensitivity of the microcapsules to dehydration are special challenges in our attempt to verify and monitor the reactions associated with this improvement. However, by means of STXM we have been able to show that both the polymerization products of SA and NVP can be mapped in the SA/NVP-modified microcapsules (Figs 6–8). The fact that, without UV irradiation, no signal for pNVP in #3 or for pSA in #4 could be detected (Fig. 6), further supports the conclusion that the photo-polymerization was essential and successful in creating the modified capsules [23]. The observed increase in calcium content in the microcapsules modified by infusion with, and polymerization of, SA in the modification process used here, is consistent with the resulting increase in the carboxylic acid content of the capsules. It should be noted that enhancement in the strength of the capsules is not simply due to an increase in  $\text{Ca}^{2+}$  concentration, as there is a significant difference in the strength of capsules formed by this polymerization route and those based on the formation of an IPN between calcium alginate and calcium polyacrylate [23].

With STXM we have mapped the distributions of Ca, alginate, pNVP and pSA, respectively (Figs 5–8). The analysis shows that the capsules have enhanced density in the outer approx. 0.5  $\mu\text{m}$  of the capsules. This is reasonable, since the  $\text{Ca}^{2+}$ , NVP and SA all diffuse into the beads from the surface to the core. During the alginate bead hydrogel formation process,  $\text{Ca}^{2+}$  is the only cross-linker for the alginate. That may be the reason that the  $\text{Ca}^{2+}$  concentration falls off gradually towards the capsule interior [41]. In contrast, the NVP evidently was concentrated only in the edge region. This may be due to (1) too short a mixing time for the reagents with the alginate beads during the polymerization step; and (2) absence of an electrical potential to drive the NVP deeper into the Ca-alginate gel. Although the same trend might be expected to occur for the distribution of acrylate, this was not the case. The results showed that the SA signal was only slightly enhanced

in the peripheral region, while a fairly uniform distribution of SA was observed throughout at least the 10–20  $\mu\text{m}$  of the peripheral region. The difference in the distribution between NVP and SAs is interesting. Quantitative analysis of the NVP and SA signals showed that the ratio of the SA to the NVP in this peripheral region is approx. 1:5 to 1:10. This is not consistent with the expected 1:1 ratio of NVP and SA in the co-polymer, and may indicate that the opportunity for NVP to contribute to the IPN polymerization is 5–10-times higher than that of SA at the periphery. A possible mechanism that may account for the deeper penetration of SA into the interior region of the capsule may be due to its ionic interaction with the  $\text{Ca}^{2+}$ . As shown in Fig. 2, the presence of SA significantly increased the amount of  $\text{Ca}^{2+}$  sequestered in the capsules, to a much greater extent than NVP. Since  $\text{Ca}^{2+}$  is expected to be dispersed throughout the capsule in the initial formation of the alginate hydrogel, this may have caused the acrylate to be distributed like-wise.

The results of this study demonstrate the power of STXM to quantitatively map the distribution of modifying reagents in alginate capsules. Through STXM we have established that there is a fundamental difference in the distribution of the polymerization products of neutral and charged monomers within the capsule. This suggests that it should be possible to use this photochemical technique to modify the outer walls of alginate capsules with a range of other neutral monomers. This approach should allow fine tuning of the surface chemistry of the capsules and also will separate the incorporated cells from possible deleterious effects associated with a radical polymerization.

### Acknowledgements

We thank Marnie Timluk and Marcia West for their superb work on sample preparation. This work was supported by an NSERC Strategic Grant (R. C., P. C.), an NSERC Major Facilities Access grant (A. P. H., R. C.) and the Canada Research Chair program (A. P. H.). The Advanced Light Source is supported by the Director, Office of Energy Research, Office of Basic Energy Sciences, Materials Sciences Division of the US Department of Energy, under Contract No. DE-AC03-76SF00098.

### REFERENCES

1. T. M. S. Chang, *Science* **146**, 524 (1964).
2. F. Lim and A. M. Sun, *Science* **210**, 908 (1980).
3. H. Wong and T. M. S. Chang, *Int. J. Artif. Organs* **16**, 731 (1986).
4. P. Aebischer, L. Wahlberg, P. A. Tresco and S. R. Winn, *Biomaterials* **12**, 50 (1991).
5. P. Aebischer, N. A. M. Pochon, B. Heyd, N. Deglon, J. M. Joseph, A. D. Zurn, E. E. Baetge, J. P. Hammang, M. Goddard, M. Lysaght, F. Kaplan, A. C. Kato, M. Schluep, L. Hirt, F. Regli, F. Porchet and N. De Tribolet, *Hum. Gene Ther.* **7**, 851 (1996).
6. P. L. Chang (Ed.), in: *Non-autologous Somatic Gene Therapy*, Chapter 12. CRC Press, Boca Raton, FL (1995).

7. J. Brauker, G. H. Frost, V. Dwarki, T. Nijjar, R. Chin, V. Carr-Brendel, C. Jasunas, D. Hodgett, W. Stone, L. K. Cohen and R. C. Johnson, *Hum. Gen. Ther.* **9**, 879 (1998).
8. A. Al-Hendy, G. Hortelano, G. S. Tannenbaum and P. L. Chang, *Hum. Gene Ther.* **6**, 165 (1995).
9. P. Aebischer, M. Schlupe, N. Déglon, J. M. Joseph, L. Hirt, B. Heyd, M. Goddard, J. P. Hammang, A. D. Zum, A. C. Kato, F. Regli and E. E. Baetge, *Nature Med.* **2**, 696 (1996).
10. J. M. Van Raamsdonk, C. J. D. Ross, M. A. Potter, S. Kurachi, K. Kurachi, D. W. Stafford and P. L. Chang, *J. Lab. Clin. Med.* **139**, 35 (2002).
11. C. J. D. Ross, L. Bastedo, S. A. Maier, M. S. Sands and P. L. Chang, *Hum. Gene Ther.* **11**, 2117 (2002).
12. C. J. D. Ross, M. Ralph and P. L. Chang, *Exp. Neurol.* **166**, 276 (2000).
13. P. Cirone, J. M. Bourgeois and P. L. Chang, *Hum. Gene Ther.* **14**, 1065 (2003).
14. D. F. Emerich, M. Plone, J. Francis, B. R. Frydel, S. R. Winn and M. D. Lindner, *Brain Res.* **736**, 99 (1996).
15. Y. Sagot, S. A. Tan, J. P. Hammang, P. Aebischer and A. C. Kato, *J. Neurosci.* **16**, 2335 (1996).
16. T. Joki, M. Machluf, A. Atala, J. Zhu, N. T. Seyfried, I. F. Dunn, T. Abe, R. S. Carroll and P. M. Black, *Nature Biotechnol.* **19**, 35 (2001).
17. T. A. Read, D. R. Sorensen, R. Mahesparan, P. O. Enger, R. Timpl, B. R. Olsen, M. H. Hjelstuen, O. Haraldseth and R. Bjerkvig, *Nature Biotechnol.* **19**, 29 (2001).
18. M. Goosen, G. O'Shea, H. Gharapetian, S. Chou and A. Sun, *Biotechnol. Bioeng.* **27**, 147 (1985).
19. M. A. Peirone, K. Delaney, J. Kwiecin, A. Fletch and P. L. Chang, *Hum. Gene Ther.* **9**, 195 (1998).
20. P. Soon-Shiong and R. E. Heintz, US Patent No. 5,792,959 (1998).
21. T. A. Becher, D. R. Kipke and T. Brandon, *J. Biomed. Mater. Res.* **54**, 76 (2001).
22. S. Schneider, P. J. Feilen, V. Slotty, D. Kampfner, S. Preuss, S. Berger, J. Bever and R. Pommer-sheim, *Biomaterials* **22**, 1961 (2001).
23. M. Wang, R. F. Childs and P. L. Chang, *J. Biomater. Sci. Polymer Edn* **16**, 91 (2005).
24. M. Wang and R. F. Childs, Patent application (2003).
25. F. Shen, C. Poncet-Legrand, S. Somers, A. Slade, C. Yip, A. M. Duft, F. M. Winnik and P. L. Chang, *Biotechnol. Bioeng.* **83**, 282 (2003).
26. H. Ade, in: *Experimental Methods In The Physical Sciences*, J. A. R. Samson and D. L. Ederer (Eds), Vol. 32, p. 225. Academic Press, San Diego, CA (1998).
27. H. Ade and S. G. Urquhart, in: *Chemical Applications of Synchrotron Radiation*, T. K. Sham (Ed.), p. 285. World Scientific Publishing, Singapore (2002).
28. H. Ade, X. Zhang, S. Cameron, C. Costello, J. Kirz and S. Williams, *Science* **258**, 972 (1992).
29. H. Ade, A. P. Smith, S. Cameron, R. Cieslinski, C. Costello, B. Hsiao, G. E. Mitchell and E. G. Rightor, *Polymer* **36**, 1843 (1995).
30. A. P. Hitchcock, I. Koprinarov, T. Tyliczszak, E. G. Rightor, G. E. Mitchell, M. T. Dineen, F. Hayes, W. Lidy, R. D. Priester, S. G. Urquhart, A. P. Smith and H. Ade, *Ultramicroscopy* **88**, 33 (2001).
31. C. Morin, H. Ikeura-Sekiguchi, T. Tyliczszak, R. Cornelius, J. L. Brash, A. P. Hitchcock, A. Scholl, F. Nolting, G. Appel, D. A. Winesett, K. Kaznacheyev and H. Ade, *J. Electr. Spectrosc. Relat. Phenom.* **121**, 203 (2001).
32. C. J. Buckley, S. Downes, N. Khaleque, S. J. Bellamy and X. Zhang, in: *Proceedings of the Annual Meeting, Microscopy Society of America*, p. 44 (1994).
33. A. P. Hitchcock, C. Morin, Y. M. Heng, R. M. Cornelius and J. L. Brash, *J. Biomater. Sci. Polymer Edn* **13**, 919 (2002).
34. J. R. Lawrence, G. D. W. Swerhone, G. G. Leppard, T. Araki, X. Zhang, M. M. West and A. P. Hitchcock, *Appl. Environ. Microbiol.* **69**, 5543 (2003).
35. I. Koprinarov, A. P. Hitchcock, W. H. Li, Y. M. Heng and H. D. H. Stover, *Macromolecules* **34**, 4424 (2001).

36. I. N. Koprinarov, A. P. Hitchcock, C. T. McCrory and R. F. Childs, *J. Phys. Chem. B* **106**, 5358 (2002).
37. B. Thu, G. Skjåk-Bræk, F. Micali, F. Vittur and R. Rizzo, *Carbohydr. Res.* **297**, 101 (1997).
38. B. Thu, O. Gaserod, D. Paus, A. Mikkelsen, G. Skjåk-Bræk, R. Toffanin, F. Vittur and R. Rizzo, *Biopolymers* **53**, 60 (2000).
39. A. L. D. Kilcoyne, T. Tylicszak, W. F. Steele, S. Fakra, P. Hitchcock, K. Franck, E. Anderson, B. Harteneck, E. G. Rightor, G. E. Mitchell, A. P. Hitchcock, L. Yang, T. Warwick and H. Ade, *J. Synchrotron Radiat.* **10**, 125 (2003).
40. T. Warwick, H. Ade, A. L. D. Kilcoyne, M. Kritscher, T. Tylicszak, S. Fakra, A. P. Hitchcock and H. A. Padmore, *J. Synchrotron Radiat.* **9**, 254 (2002).
41. N. P. Desai, P. Soon-Shiong, P. A. Sandford and R. E. Heintz, US Patent No. 5,334,640 (1992).